AUT Journal of Mechanical Engineering

AUT J. Mech. Eng., 6(3) (2022) 363-386
DOI: 10.22060/ajme.2022.20964.6026

Design of Robust Proportional-(Proportional-Derivative) Controller for an Autonomous Underwater Vehicle Using Quantitative Feedback Theory in the Diving Plane

F. Safari[1], M. Rafeeyan[1]*, M. Danesh[2]

[1] Department of Mechanical Engineering, Yazd University, Yazd, Iran
[2] Department of Mechanical Engineering, Isfahan University of Technology, Isfahan, Iran

ABSTRACT: In this paper, a robust proportional-(proportional-derivative) controller is designed for an autonomous underwater vehicle using quantitative feedback theory in the presence of plant uncertainty and disturbances in diving plane motion. The controller is designed in cascade feedback in the presence of parametric uncertainty, ocean currents, sea waves, and fin error. The proportional-derivative controller controls the angle of the vehicle pitch and an outer proportional loop controller will control the vehicle depth. Since using classical methods to adjust proportional-derivative for the inner loop and proportional for the outer loop, despite the plant uncertainty and the presence of disturbances, is complex and time-consuming. therefore, the quantitative feedback theory technique, as a robust controller method, is used in this research. System stability is considered in the design process. All design steps are based on linearized equations of motion but the performance of the proportional-(proportional-derivative) controller designed by the robust quantitative feedback theory method is simulated numerically for nonlinear dynamic equations of motion. The simulation results show that the designed proportional-(proportional-derivative) controller using quantitative feedback theory offers robust stability, disturbance rejection, and proper reference tracking over a range of autonomous underwater vehicle parametric uncertainties.

Review History:

Received: Jan. 08, 2022
Revised: May, 07, 2022
Accepted: Jun. 08, 2022
Available Online: Jun. 20, 2022

Keywords:

Autonomous underwater vehicle
proportional-(proportional-derivative) control
Quantitative feedback theory

1- Introduction

An Autonomous Underwater Vehicle (AUV) is an unmanned submersible in different sizes. There are many applications for AUVs, including the oil industry, pipeline surveillance, high-risk waters operations, environmental monitoring, seabed mapping, rescue operations, and so on [1]. To perform these operations, the AUV needs to be well controlled by the operator, but its control is fraught with challenges. The main problems of the AUV control are parametric uncertainties (added mass, hydrodynamic coefficients, etc.), nonlinear and coupled dynamics, and disturbances caused by ocean currents and sea waves [1, 2].

Over the past few decades, various control methods for controlling AUVs such as Proportional-Derivative Controller (PD) [3], Proportional-Integral-Derivative Controller (PID) [4], Static Feedback Controller [5], Sliding Mode Controller (SMC) [6], Backstepping Controller (BSC) [7], Predictive Controller [8], Adaptive Controller [9], Fuzzy Logic Controller (FLC) [10], Neural Network Controller (NNC) [11] etc. have been extensively researched. Since almost all control methods have advantages and disadvantages, it is possible to achieve a suitable controller by intelligently combining several controllers.

PD and PID are the most widely used controllers due to their simplicity of design and good performance. However, it is well-known that when the plant's dynamics are faced with structural uncertainty and input and output disturbances, the performance of the PID controller is often degraded. The impact of these drawbacks can be reduced by using other control strategies such as robust controllers. Inspired by this issue, several advanced PD/PID control schemes for underwater vehicles have been proposed in previous research and some of them are mentioned. According to some research, the optimal adjustment process of the PID controllers is time-consuming. As a result, methods for adjusting PID gains have been developed in recent years. In Ref. [12], a Cloud-Model-Based Quantum Genetic Algorithm (CQGA) was used to tune the gains of a fractional order PID for set point regulation in the direction, depth, and tracking of the AUV. In addition, it is shown that the closed-loop fraction order system is stable. By comparing the simulations and experiments, satisfactory performance was obtained from the index of overshooting value, settling time, and steady-state error. In Ref. [13], the proportional-integral-derivative control (PID) parameters have been optimized using the Particle Swarm Optimization (PSO) method to control underwater vehicles. The gains of the PID controller are tuned for a specific path, but in Ref. [14]using fuzzy logic, the controlling interest is adapted to change the path. A simulation has been performed to confirm

*Corresponding author's email: rafeeyan@yazd.ac.ir

the adaptive nature of the fuzzy PID controller. In [15], Fuzzy logic has been used to improve the PID controller in order to path following and robustness to output disturbance. The motion of AUV, in naval missions, could be disrupted by ocean currents or a sudden change in its physical parameters. To overcome these problems, adaptive controllers can be used as a suitable solution for AUV control. The main feature of the adaptive controller is its ability to update control gains based on changes in plant dynamics and output disturbances. As an example of this method, an adaptive PD controller has been proposed for the set point regulation in Ref [16]. The law of control includes PD plus buoyancy compensation (PD+) with an adaptive term that estimates and compensates for the uncertainty of parameters and output disturbances.

In summary, fuzzy approaches and intelligent algorithms such as PSO and Genetic Algorithm (GA) used to adjust PID control can be useful to achieve good control performance. However, the ability of these methods to deal with parametric uncertainty and large changes in environmental conditions is weak. One of the most important disadvantages of linear controllers such as Linear Quadratic Regulator (LQR) and Linear–Quadratic–Gaussian (LQG) is that they cannot consider system nonlinearities, so they can affect the optimal performance and even the issue of stability in high maneuvers [2]. The neural network also has weaknesses that affect its functionality. This method converges at a low rate over a long training period, which is not acceptable in some systems. Also, a classical neural network does not qualify for the main requirements such as fast response and less overshoot [2]. FLC is easy to use in industrial processes due to its simple control structure, and easy and cost-effective design. However, to control systems with high uncertainty and nonlinearity, FLC with fixed scaling factors and fuzzy rules may not work perfectly. If the system does not have an inherent integrating property, traditional FLC can have an error at a steady state [2]. SMC control is an old method that is a good solution for nonlinear systems but can cause chattering on actuators, increase electrical power consumption, and make faults on fins [1]. In the case of adaptive controllers, their main advantages are the automatic adjustment of the gains as well as the need for only minor details of the vehicle mathematical model. However, the disadvantage of this method is the low rate of gain adjustment and overestimation of feedback gain [4]. Modern controllers are more robust to dynamic changes and can provide better performance indicators than conventional controllers. However, they may require complete accurate models. Most of these methods mentioned to improve PID type controllers complicate the design as well as the implementation of this controller and eliminate or undermine the benefits of its simplicity. Due to these drawbacks, the Quantitative Feedback Theory (QFT) method is proposed to adjust the gain of PID controllers to overcome the shortcomings of previous algorithms for AUV.

The main purpose of this paper is to use the QFT quantitative feedback theory method for tuning PD controller gains for the control of the inner pitch loop and the P controller gain to control the outer depth loop in a cascade feedback system to control the depth of an AUV in diving plane motion in the presence of parametric uncertainty, ocean currents, sea waves, and fin error. The following steps are pursued in this research:

1 .Modeling the dynamics of SAED-AUV motion and deriving its transfer functions, modeling sea wave as output disturbance, modeling ocean currents as parametric uncertainty in the depth transfer function, and modeling fin error as input disturbance.

2 .Achieve a classic, simple, and operational PID controller, but at the same time robust to parametric uncertainty, environmental disturbances, and fin error.

3. Tuning of P-PD controller gains based on the QFT method in the presence of parametric uncertainty, environmental disturbances, and fin error for an AUV.

4 .Stabilizing of inner pitch loop and outer depth loop in the presence of parametric uncertainty and hydrodynamic coefficients errors.

5 .Reduction of the effect of environmental disturbances and fin and on the optimal performance of the system and tracking the reference input.

6. Simulation of depth controller (P-PD) performance despite parametric uncertainty, environmental disturbances, fin error, and saturation of rate and value of horizontal fin angle and analysis of the system in response to depth reference input and disturbances.

The QFT method is one of the robust control methods that was first introduced for linear systems and then extended for nonlinear systems. Compared to other robust control methods based on optimization, QFT has advantages such as a) the ability to quantitatively evaluate the feedback cost, b) the ability to consider phase information in the design process, and c) the ability to provide design transparency. Much research [17-20] has been done to adjust the gains of PID controllers using the QFT method.

This paper is organized as follows: A description of the dynamic model of the underwater vehicle, its linearization in the depth plane, and a description of the type of environmental disturbances are given in Section 2. Then, the proposed control method whose structure is an inner proportional and derivative (PD) pitch loop, and an outer proportional depth loop in a cascade feedback system to control the depth of an AUV is given. Next, parametric uncertainty, ocean currents, sea waves, and fin error are modeled and the gain of the controllers is then extracted by the QFT method, which is described in Section 3. The control block diagram is designed in a Simulink toolbox and the SAED-AUV response is simulated in the presence of parametric uncertainty, environmental disturbance, and fin constraints to track the reference depth input, which is discussed in Section 4. Section 4 presents the design results and in Section 5 the conclusions of this research will be presented.

2- Mathematical Model of The Underwater Vehicle Motion

The underwater vehicle has 6 degrees of freedom. Therefore, 6 independent coordinates are needed to

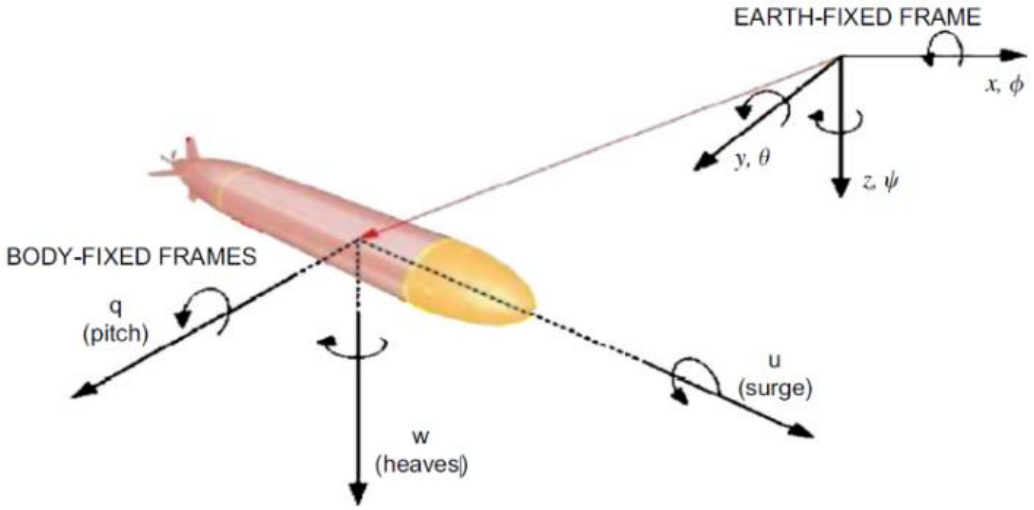

Fig. 1. AUV body frame and inertial reference frame

Table 1. Notation for underwater vehicle

Dof	Motion	Forces and moments	Linear and angular velocity	Positions and Euler angels
1	Surge	$X(\mathrm{N})$	$u(\mathrm{m/s})$	$x(\mathrm{m})$
2	Sway	$Y(\mathrm{N})$	$v(\mathrm{m/s})$	$y(\mathrm{m})$
3	Heave	$Z(\mathrm{N})$	$w(\mathrm{m/s})$	$z(\mathrm{m})$
4	Roll	$K(\mathrm{Nm})$	$p(\mathrm{rad/s})$	$\varphi(\mathrm{rad})$
5	Pitch	$M(\mathrm{Nm})$	$q(\mathrm{rad/s})$	$\theta(\mathrm{rad})$
6	Yaw	$N(\mathrm{Nm})$	$r(\mathrm{rad/s})$	$\psi(\mathrm{rad})$

determine the position and direction of the vehicle. The first 3 coordinates and their time derivatives are used for linear position and motion, and the last 3 coordinates and their time derivatives express motion and direction angles. The names of the movements, the applied forces, the speed, and the position of each movement are expressed in Table 1.

A proper definition of coordinate systems is necessary to determine the physical behavior of an underwater vehicle. There are two coordinate systems that must be understood independently in this connection: the global or fixed coordinate system, and the moving or body-fixed coordinate system. The global coordinate system is defined in relation to the earth and is also sometimes referred to as the reference earth coordinate system or inertial coordinate system. The origin of the inertial coordinate system is usually considered at sea level. The two axes x and y are at sea level, corresponding to the north and east, and the z-axis is considered in the direction of the depth of the sea.

The moving coordinate system is defined relative to the body of the underwater vehicle under consideration and is known as the body coordinate system. The origin of the body coordinate system is usually either in the center of buoyancy (CB), where the vehicle center is the displaced center of volume of the submerged vehicle or in the center of gravity (CG), where the center of gravity is the center of gravity of the underwater vehicle. The x_b axis is in the direction of the longitudinal axis and towards the nose, the y_b axis is in the right direction and the z_b axis is considered according to the law of the right hand.

Two coordinate frames are shown in Fig. 1. Six velocity components [u, v, w, p, q, and r]$^{\mathrm{T}}$ are defined in the body fixed frame, while the earth-fixed frame defines the corresponding attitudes and positions [x, y, z, ϕ, θ, and ψ]$^{\mathrm{T}}$. It is listed in Table 1.

The kinematics transformation matrix between the vehicle's velocity in Body-frame and position in Earth-frame (World frame) is as follows:

$$[\mathbf{R}]=[\mathbf{R}]_{z,\psi}[\mathbf{R}]_{y,\theta}[\mathbf{R}]_{x,\varphi}$$

$$=\begin{bmatrix}\cos\psi & -\sin\psi & 0\\ \sin\psi & \cos\psi & 0\\ 0 & 0 & 1\end{bmatrix}.\begin{bmatrix}\cos\theta & 0 & \sin\theta\\ 0 & 1 & 0\\ -\sin\theta & 0 & \cos\theta\end{bmatrix}\begin{bmatrix}1 & 0 & 0\\ 0 & \cos\varphi & -\sin\varphi\\ 0 & \sin\varphi & \cos\varphi\end{bmatrix}$$

$$[\mathbf{R}]=\begin{bmatrix}\cos\theta\cos\psi & \sin\varphi\sin\theta\cos\psi-\cos\varphi\sin\psi & \cos\varphi\sin\theta\cos\psi+\sin\varphi\sin\psi\\ \cos\theta\sin\psi & \sin\varphi\sin\theta\sin\psi+\cos\varphi\cos\psi & \cos\varphi\sin\theta\sin\psi-\sin\varphi\cos\psi\\ -\sin\theta & \sin\varphi\cos\theta & \cos\varphi\cos\theta\end{bmatrix} \quad (1)$$

$$[\mathbf{T}]=\begin{bmatrix}1 & \sin\varphi\tan\theta & \cos\varphi\tan\theta\\ 0 & \cos\varphi & -\sin\varphi\\ 0 & \sin\varphi\sec\theta & \cos\varphi\sec\theta\end{bmatrix} \quad (2)$$

All velocity components can be defined in groups in vector forms as follows:

$$[\mathbf{V}]_{body}=\begin{bmatrix}u\\ v\\ w\\ p\\ q\\ r\end{bmatrix} \quad (3)$$

$$[\mathbf{V}]_{world}=\begin{bmatrix}\dot{x}\\ \dot{y}\\ \dot{z}\\ \dot{\varphi}\\ \dot{\theta}\\ \dot{\psi}\end{bmatrix} \quad (4)$$

Therefore, the matrix for converting velocities of body coordinates to world coordinates is as follows:

$$[\mathbf{V}]_{world}=\begin{bmatrix}[\mathbf{R}] & \mathbf{0}\\ \mathbf{0} & [\mathbf{T}]\end{bmatrix}[\mathbf{V}]_{body} \quad (5)$$

2- 1- Dynamic equations of motion of an underwater vehicle

Using Newton's laws, the dynamics of the AUV as a rigid body with 6 degrees of freedom are obtained as follows:

$$\begin{aligned}&m\mathbf{a}=\Sigma\mathbf{F}\\ &\mathbf{I}\boldsymbol{\alpha}=\Sigma\mathbf{M}\end{aligned} \quad (6)$$

By expanding the force and moment equations, dynamic equations of the AUV in the body frame are obtained as follows:

$$\begin{aligned}
&m\begin{bmatrix}\dot{u}-\upsilon r+wq-x_G\left(q^2+r^2\right)+\\ y_G\left(pq-\dot{r}\right)+z_G\left(pr+\dot{q}\right)\end{bmatrix}=X\\
&m\begin{bmatrix}\dot{\upsilon}-wq+ur-y_G\left(r^2+p^2\right)+\\ z_G\left(qr-\dot{p}\right)+x_G\left(qp+\dot{r}\right)\end{bmatrix}=Y\\
&m\begin{bmatrix}\dot{w}-uq+\upsilon p-z_G\left(p^2+q^2\right)+\\ x_G\left(rp-\dot{q}\right)+y_G\left(rq+\dot{p}\right)\end{bmatrix}=Z\\
&I_x\dot{p}+\left(I_z-I_y\right)qr-I_{xz}\left(\dot{r}+pq\right)+\\
&I_{yz}\left(r^2-q^2\right)+I_{xy}\left(pr-\dot{q}\right)+\\
&m\left[y_G\left(\dot{w}-uq+\upsilon p\right)-z_G\left(\dot{\upsilon}-wp+ur\right)\right]=K\\
&I_y\dot{q}+\left(I_x-I_z\right)rp-I_{xy}\left(\dot{p}+qr\right)+\\
&I_{xz}\left(p^2-r^2\right)+I_{yz}\left(qp-\dot{r}\right)+\\
&m\left[z_G\left(\dot{u}-\upsilon r+wq\right)-x_G\left(\dot{w}-uq+\upsilon p\right)\right]=M\\
&I_z\dot{r}+\left(I_y-I_x\right)pq-I_{yz}\left(\dot{q}+rp\right)+\\
&I_{xy}\left(q^2-p^2\right)+I_{xz}\left(rq-\dot{p}\right)+\\
&m\left[x_G\left(\dot{\upsilon}-wp+ur\right)-y_G\left(\dot{u}-\upsilon r+wq\right)\right]=N
\end{aligned} \quad (7)$$

where *X, Y, Z, K, M,* and *N* are external forces and moments on the AUV body. These forces can be obtained by expanding the force and moment components created by the hydrodynamic and hydrostatic forces and the external forces resulting from the control surface and thrust of the propellers. It can be shown that these forces and torques are as follows [21]:

$$\begin{aligned}
X=&-\left(W-B\right)\sin\theta+X_{u|u|}|u|u+\\
&X_{\dot{u}}\dot{u}+X_{vr}vr+X_{wq}wq+\\
&X_{qq}q^2+X_{rr}r^2+X_{Propulsion}\\
Y=&\left(W-B\right)\cos\theta\sin\phi+Y_{v|v|}|v|v+\\
&Y_{r|r|}|r|r+Y_{\dot{v}}\dot{v}+Y_{\dot{r}}\dot{r}+Y_{uvl}uv+\\
&Y_{ur}ur+Y_{wp}wp+Y_{pq}pq+Y_{uu\delta r}u^2\delta_r\\
Z=&\left(W-B\right)\cos\theta\cos\phi+Z_{w|w|}|w|w+\\
&Z_{q|q|}|q|q+Z_{\dot{w}}\dot{w}+Z_{\dot{q}}\dot{q}+Z_{uw}uw+\\
&Z_{uq}uq+Z_{vp}vp+Z_{rp}rp+Z_{uu\delta e}u^2\delta_e
\end{aligned} \quad (8)$$

$$K = \left(y_G W - y_B B\right)cos\theta cos\phi -$$

$$\left(z_G W - z_B B\right)cos\theta sin\phi +$$

$$K_{p|p|}\left|p\right|p + K_{\dot{p}}\dot{p} + K_{Propulsion}$$

$$M = -\left(z_G W - z_B B\right)sin\theta -$$
$$\left(x_G W - x_B B\right)cos\theta cos\phi +$$
$$M_{w|w|}\left|w\right|w + M_{q|q|}\left|q\right|q + M_{\dot{w}}\dot{w} +$$
$$M_{\dot{q}}\dot{q} + M_{uw}uw + M_{uq}uq +$$
$$M_{vp}vp + M_{rp}rp + M_{uu\delta e}u^2\delta_e$$

$$N = \left(x_G W - x_B B\right)cos\theta sin\phi +$$
$$\left(y_G W - y_B B\right)sin\theta + N_{v|v|}\left|v\right|v +$$
$$N_{r|r|}\left|r\right|r + N_{\dot{v}}\dot{v} + N_{\dot{r}}\dot{r} + N_{uv}uv +$$
$$N_{ur}ur + N_{wp}wp + N_{pq}pq + N_{uu\delta r}u^2\delta_r$$

The right hand side terms of Eq. (8) are initiated from eight force and moment groups: hydrostatic forces and moments due to weight W and buoyancy B, hydrodynamic damping coefficients ($X_{u|u|}$, $Y_{v|v|}$, $Y_{r|r|}$, $Z_{w|w|}$, $Z_{q|q|}$, $K_{p|p|}$, $M_{w|w|}$, $M_{q|q|}$, $N_{v|v|}$ and $N_{r|r|}$), added mass coefficients ($X_{\dot{u}}$, $Y_{\dot{v}}$, $Y_{\dot{r}}$, $Z_{\dot{w}}$, $Z_{\dot{q}}$, $K_{\dot{p}}$, $M_{\dot{w}}$, $M_{\dot{q}}$, $N_{\dot{v}}$ and $N_{\dot{r}}$), coupled added mass coefficients (X_{vr}, X_{wq}, X_{qq}, X_{rr}, Y_{wp}, Y_{pq}, Z_{vp}, Z_{rp}, M_{vp}, M_{rp}, N_{wp} and N_{pq}), hydrodynamic coefficients of the body lift, control surface and Munk moment (M_{uw} and N_{uv}), hydrodynamic coefficients of the body lift and control surface (Y_{uv} and Z_{uw}), hydrodynamic coefficients of force and moment obtained from control surface angle ($Y_{uu\delta r}$, $Z_{uu\delta e}$, $M_{uu\delta e}$ and $N_{uu\delta r}$), and the thrust and moment of the propellers ($X_{Propulsion}$ and $K_{Propulsion}$).

2- 2- Equations of motion in the depth plane

Using Eq. (5) and dynamic equations Eqs. (7) and (8) and assuming zero for other degrees of freedoms except for depth plane, the equations of motion in the depth plane are extracted as follows:

$$m\left[\dot{u} + wq - x_G q^2 + z_G\dot{q}\right] =$$
$$-\left(W - B\right)sin\theta + X_{u|u|}\left|u\right|u +$$
$$X_{\dot{u}}\dot{u} + X_{wq}wq + X_{qq}q^2 + X_{Propulsion}$$

$$m\left[\dot{w} - uq - z_G q^2 - x_G\dot{q}\right] =$$
$$\left(W - B\right)cos\theta + Z_{w|w|}\left|w\right|w +$$
$$Z_{q|q|}\left|q\right|q + Z_{\dot{w}}\dot{w} + Z_{\dot{q}}\dot{q} +$$
$$Z_{uw}uw + Z_{uq}uq + Z_{uu\delta e}u^2\delta_e \qquad (9)$$

$$I_y\dot{q} + m\left[z_G\left(\dot{u} + wq\right) - x_G\left(\dot{w} - uq\right)\right] =$$
$$-\left(z_G W - z_B B\right)sin\theta - \left(x_G W - x_B B\right)cos\theta +$$
$$M_{w|w|}\left|w\right|w + M_{q|q|}\left|q\right|q + M_{\dot{w}}\dot{w} + M_{\dot{q}}\dot{q} +$$
$$M_{uw}uw + M_{uq}uq + M_{uu\delta e}u^2\delta_e$$

$$\dot{x} = u\cos\theta + w\sin\theta$$

$$\dot{z} = -u\sin\theta + w\cos\theta$$

$$\dot{\theta} = q$$

The nonlinear equations of the SAED vehicle in the depth plane and the operating speed range are simplified as follows:

$$m\left[\dot{u} + wq - x_G q^2 + z_G\dot{q}\right] =$$
$$-\left(W - B\right)sin\theta + X_{u|u|}\left|u\right|u +$$
$$X_{\dot{u}}\dot{u} + X_{Propulsion}$$

$$m\left[\dot{w} - uq - z_G q^2 - x_G\dot{q}\right] =$$
$$\left(W - B\right)cos\theta + Z_{\dot{w}}\dot{w} + Z_{\dot{q}}\dot{q} +$$
$$Z_{uw}uw + Z_{uq}uq + Z_{uu\delta e}u^2\delta_e \qquad (10)$$

$$I_y\dot{q} + m\left[z_G\left(\dot{u} + wq\right) - x_G\left(\dot{w} - uq\right)\right] =$$
$$-\left(z_G W - z_B B\right)sin\theta - \left(x_G W - x_B B\right)cos\theta +$$
$$M_{\dot{w}}\dot{w} + M_{\dot{q}}\dot{q} + M_{uw}uw + M_{uq}uq + M_{uu\delta e}u^2\delta_e$$

$$\dot{x} = u\cos\theta + w\sin\theta$$

$$\dot{z} = -u\sin\theta + w\cos\theta$$

$$\dot{\theta} = q$$

2- 3- Linearization of the AUV equations of motion in the depth plane

Based on the following assumptions we can linearize the equations of motion:

small vehicle perturbations about $\theta = 0$

vehicle motion consists of small perturbations around a steady point (U,0,0)

use the Maclaurin expansion of the trigonometric terms $u \ll U,\ U > 0$

dropping any higher-order terms

Then, equations of motion in the depth plane are linearized as follows [21]:

$$\left(m - X_{\dot{u}}\right)\dot{u} - mz_G\dot{q} -$$
$$X_u u - X_q q - X_\theta\theta = 0$$

$$\left(m - Z_{\dot{w}}\right)\dot{w} - \left(mx_G + Z_{\dot{q}}\right)\dot{q} -$$
$$Z_w w - \left(mU + Z_q\right)q = Z_{\delta_s}\delta_s \qquad (11)$$

$$-\left(mx_G + M_{\dot{w}}\right)\dot{w} + \left(I_y - M_{\dot{q}}\right)\dot{q} -$$
$$M_w w + \left(mUx_G - M_q\right)q - M_\theta\theta = M_{\delta_s}\delta_s$$

Table 2. NATO Sea State Numeral Table

Sea state	Characteristics	Significant wave height (m)	Wave period (sec)
0	Calm (glassy)	0	-
1	Calm (rippled)	0-0.1	-
2	Smooth	0.1-0.5	0.84
3	Slight	0.5-1.25	0.84
4	Moderate	1.25-2.5	0.71
5	Rough	2.5-4	0.65

$$\dot{x} = u + w\theta$$
$$\dot{z} = w - U\theta$$
$$\dot{\theta} = q$$

Assuming that z_G and heave velocity are small compared to the other components, we can first separate the heave and pitch equations from the surge and using the second hypothesis and assuming $x_G = 0$, simplify the equations of motion in the form of a state matrix as follows:

$$\begin{bmatrix} \dot{q} \\ \dot{z} \\ \dot{\theta} \end{bmatrix} = \begin{bmatrix} \frac{M_q}{I_y - M_{\dot{q}}} & 0 & \frac{M_\theta}{I_y - M_{\dot{q}}} \\ 0 & 0 & -U \\ 1 & 0 & 0 \end{bmatrix} \begin{bmatrix} q \\ z \\ \theta \end{bmatrix} + \begin{bmatrix} \frac{M_{\delta_s}}{I_y - M_{\dot{q}}} \\ 0 \\ 0 \end{bmatrix} \begin{bmatrix} \delta_s \end{bmatrix} \quad (12)$$

2- 4- Environmental disturbances

Environmental factors such as ocean currents causing a disturbance at sea and can be considered as linear velocities in all directions ($[u_c, v_c$ and $w_c]^T$) and at sea depth (z). Ocean currents cause a relative velocity when the speed of an underwater vehicle is recorded by accelerometer sensors, resulting in a disturbance in the actual velocity of the vehicle. This disturbance can be considered as a parametric uncertainty in the velocity in the depth transfer function (G_z).

Sea waves are another environmental factor that causes disturbance to AUV motion. Modeling these waves and including them in an AUV model is complex. These sea waves create peaks and bottoms at the calm surface of the sea, and a pressure sensor records permanent turbulence proportional to the height of the wave relative to the calm surface of the sea. These oscillations cause the control system of AUV continuously commands depth stabilization and creates parallel motion of this sea wave. In this research, the sea level changes, as a disturbance, is assumed as follows:

$$z_{disturb} = \frac{H_{1/3}}{2} sin\left(\frac{2\pi}{T} t\right) \quad (13)$$

which is a function of time, and $H_{1/3}$ is equal to the significant wave height and T is the corresponding wave period, which are determined from sea conditions according to Table 2. This perturbation is added to the system as output disturbance.

The angle error of the control surface (horizontal stern plane), which is due to the looseness of the connection of the fin to the drive mechanism and the accuracy of the servomotor, can be considered as $V(t) = 0.5$ deg. This error is added to the system as input disturbance.

2- 5- AUV specifications

The underwater vehicle discussed in this article is an AUV called SAED. It has only one propeller fixed in the tail, and four control fins are mounted in the form of a cruciform shape near the tail (Figs. 3 and 4). The hull shape of the SAED vehicle (as shown in Fig. 2) is based on the Myring hull profile equations as follows [21, 22]:

The shape of the nose is given by the modified semi-elliptical radius distribution:

$$r(\Xi) = \frac{1}{2} d \left[1 - \left(\frac{\Xi + a_{Offset} - a}{a}\right)^2\right]^{\frac{1}{n}} \quad (14)$$

The geometry of the tail is given by the equation:

$$r(\Xi) = \frac{1}{2} d - \left[\frac{3d}{2c^2} - \frac{\tan\theta}{c}\right](\Xi - l_f)^2 + \left[\frac{d}{c^3} - \frac{\tan\theta}{c^2}\right](\Xi - l_f)^3 \quad (15)$$

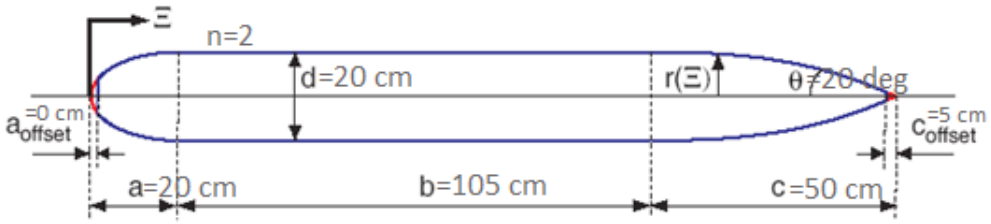

Fig. 2. Myring hull profile [21, 22] and SAED dimension specification

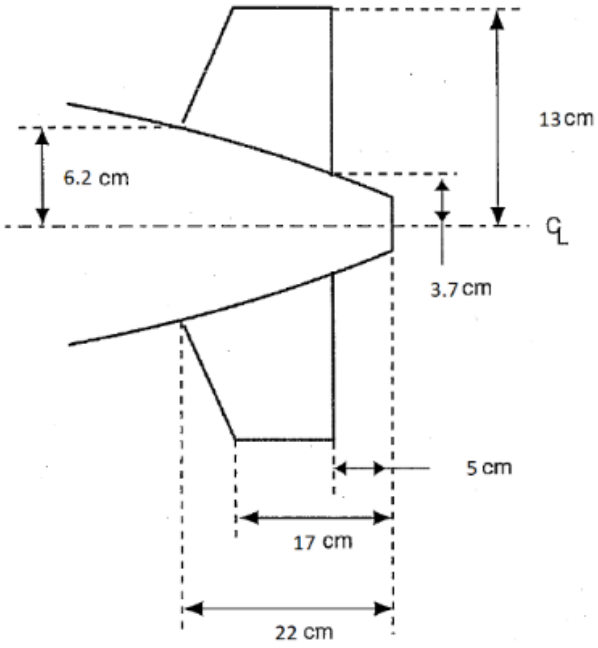

Fig. 3. SAED plane specifications

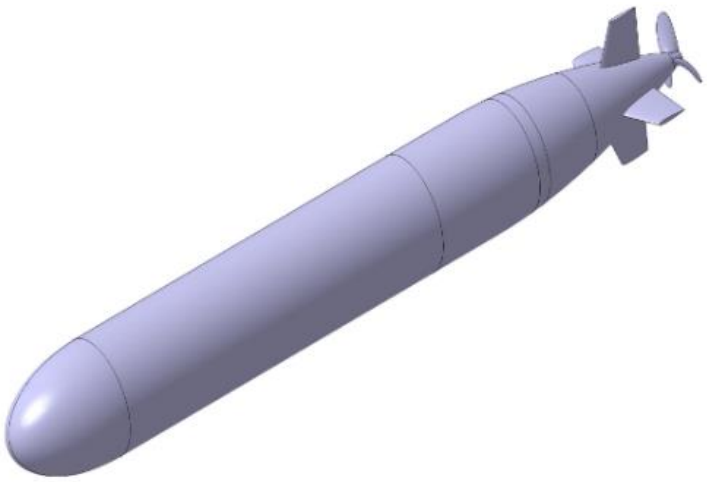

Fig. 4. 3D SAED-AUV

Table 3. Numerical values of the AUV (linear model) parameters for nominal plant (SAED-AUV)

Parameter	Parameter definition	Value	Unit
L	Vehicle length	1.780	m
m	Vehicle mass	45.89	kg
CG	The vertical distance from the center of mass to the center of buoyancy	0.018	m
M_q	Hydrodynamic moment coefficient around the lateral axis of the body due to the angular velocity around the lateral direction	-20.059	kg.m^2/s
$M_{\dot{q}}$	Added mass moment around the lateral axis of the body due to the angular velocity around the lateral direction	-6.090	kg.m^2
M_{δ_s}	Hydrodynamic moment coefficient around the lateral axis of the body due to the angle of the horizontal fin	35.422	kg.m^2/s^2
M_θ	Righting moment coefficient	-8.103	kg.m^2/s^2
I_y	Mass inertia moment around the lateral axis of the body	9.002	kg.m^2
U	Total movement speed	1.543	m/s

$$l_f = a + b - a_{Offset} \tag{16}$$

The hydrodynamic characteristics and required data of the vessel for the controller design are shown in Table 3.

3- Control System Design

Using the state equations developed for the three-term state vector model, Eq. (12), a simple vehicle controller is designed, consisting of an inner Proportional-Derivative (PD) pitch loop, and an outer proportional depth loop, which are described below:

3- 1- Vehicle transfer functions

The first step in designing a vehicle control system is to derive its transfer functions. First, the inner pitch loop transfer function, the ratio of the input angle of the horizontal stern control surfaces δ_s to the output angle of the vehicle pitch θ, is obtained. Taking the Laplace transform of Eq. (12), the open-loop transfer function for the inner pitch loop can be derived as follows:

$$G_\theta = \frac{\theta(s)}{\delta_s(s)} = \frac{\dfrac{M_{\delta_s}}{I_y - M_{\dot{q}}}}{s^2 - \dfrac{M_q}{I_y - M_{\dot{q}}}s - \dfrac{M_\theta}{I_y - M_{\dot{q}}}} \tag{17}$$

In the next step, the outer depth loop transfer function is calculated, which relates the input angle of the vehicle pitch θ to the output depth of the vehicle z. In real conditions, the response of the inner pitch loop is fast enough compared to the outer depth loop so that the desired pitch θ_d of the vehicle can be considered the same as the actual vehicle pitch θ. According to the linear kinematic and dynamic equations, taking the Laplace transform of Eq. (12), the depth transfer function is obtained as follows:

$$G_z = \frac{z(s)}{\theta(s)} = -\frac{U}{s} \tag{18}$$

3- 2- Control law

The control law for the inner loop (pitch control) is considered as a proportional-derivative controller PD in the form of Eq. (19) and modified by a low-pass filter in the form of Eq. (20) as follows:

$$\frac{\delta_s(s)}{e_\theta(s)} = -K_P(\tau_D s + 1) \tag{19}$$

$$\frac{\delta_s(s)}{e_\theta(s)} = -K_P\frac{(\tau_D s + 1)}{(0.1\tau_D s + 1)} \tag{20}$$

where $e_\theta(s) = \theta_d - \theta$, K_P is the proportional gain, and τ_D is the derivative time constant in seconds.

There is a minus sign applied to the proportional gain due to the difference in sign conventions between the stern plane angle and vehicle pitch angle. A positive stern plane angle will generate a negative moment about the y-axis, forcing the

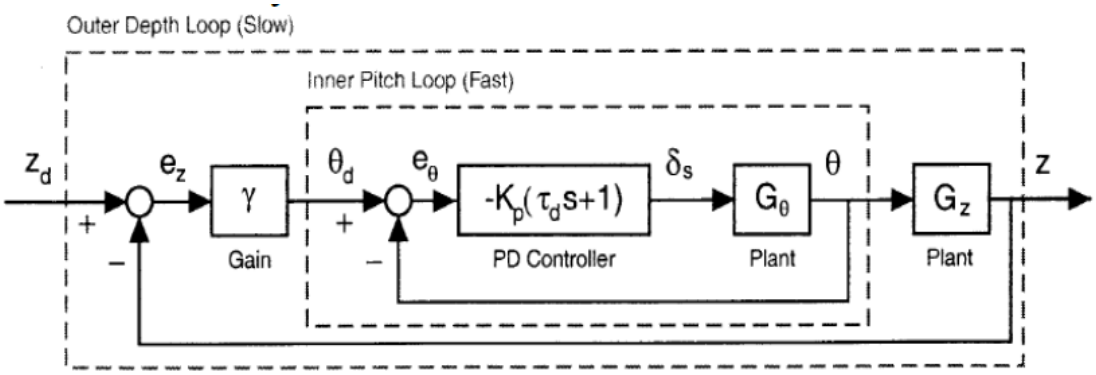

Fig. 5. Block diagram of the AUV control system in the depth plane

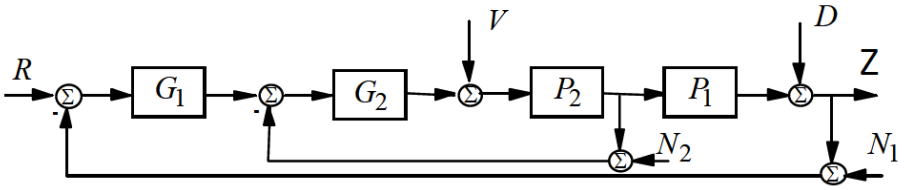

Fig. 6. Two-loop cascade feedback system

vehicle to pitch down (negative pitch rate).

The control law for the outer loop can be expressed as:

$$\frac{\theta(s)}{e_Z(s)} = \gamma \tag{21}$$

where $e_z(s) = z_d - z$ and γ is the proportional gain of the depth control loop.

After extracting the vehicle transfer functions in the depth plane and defining the pitch and depth control laws, the block diagram of the AUV control system in the diving plane is described in Fig. 5.

3- 3- Determination of controller gain using the QFT method

The QFT method is one of the robust control methods that was first introduced for linear systems and then developed for nonlinear systems. QFT emphasizes the use of feedback to obtain system performance despite the uncertainty in the process and the disturbances involved. The main idea of this method is that in the absence of uncertainty in the system, even for stabilization, no feedback is needed, but in practice most processes have uncertainty. Therefore, the use of feedback is essential and it is the controller's task to generate the required amount of feedback at all times.

By introducing parametric uncertainties and input disturbance to the motion dynamics, the block diagram of the control system of Fig. 5 can be considered as a two-loop cascade feedback system in the form of a new block diagram as in Fig. 6.

where P_2 and P_1 are plant transfer functions with parametric uncertainty and they are the same as G_θ (pitch transfer function) and G_z (depth control transfer function), respectively. Considering the 20% error in determining the values of hydrodynamic coefficients and the 20% error due to the effect of ocean currents on velocity, these functions are defined as follows:

$$\mathcal{P}_2 = \left\{ \begin{array}{l} P_2 = \dfrac{\dfrac{M_{\delta_s}}{I_y - M_{\dot{q}}}}{s^2 - \dfrac{M_q}{I_y - M_{\dot{q}}} s - \dfrac{M_\theta}{I_y - M_{\dot{q}}}} : \\ M_{\delta_s}\left(M_q, M_\theta, I_y, M_{\dot{q}}\right) \epsilon \left[0.8\ 1.2\right] \times \\ M_{\delta_s N}\left(M_{qN}, M_{\theta N}, I_{yN}, M_{\dot{q}N}\right) \end{array} \right\} \tag{22}$$

$$\mathcal{P}_1 = \left\{ P_1 = -\frac{U}{s} : U \epsilon \left[0.8\ 1.2\right] \times U_N \right\}$$

The values of the parameters $M_{\delta_s N}$ and etc. in Eq. (22) are the nominal values of the SAED vehicle linear model and are given in Table3 .

The controller design problem is to adjust the gain of the two controllers $G_2 = -K_P(\tau_D s+1)$ and $G_1 = \gamma$ using the quantitative feedback theory method. By defining the closed loop transfer function for the inner pitch loop as $T_2(s) = \left|\frac{P_2(s)G_2(s)}{1+P_2(s)G_2(s)}\right|$ and the outer loop transfer function as $P_{12}(s) = T_2(s)P_1(s)$ and then defining the outer loop transfer function as depth control $T_1(s) = \left|\frac{P_{12}(s)G_1(s)}{1+P_{12}(s)G_1(s)}\right|$, the design steps are done during the following process:

The inner loop (pitch): For the inner loop, only the robust stability of the system is important

The inner closed-loop system should be robust and stable with at least a 50° phase margin for all $P_2 \epsilon \mathcal{P}_2$

$$\left|\frac{P_2(s)G_2(s)}{1+P_2(s)G_2(s)}\right| \le 1.2 \ , \quad \omega \epsilon [0\ 1000]\left(\frac{rad}{s}\right) for\ P_2 \epsilon \mathcal{P}_2 \tag{23}$$

Outer loop (depth): The purpose of this research is first the robust stability of the system, depth control, and good performance of the system in tracking the reference input and then rejecting disturbances.

The inner closed-loop system should be robust and stable with at least a 50°phase margin for all $P_1 \epsilon \mathcal{P}_1$ and $P_2 \epsilon \mathcal{P}_2$

$$\left|\frac{P_{12}(s)G_1(s)}{1+P_{12}(s)G_1(s)}\right| \le 1.2 \ , \quad \omega \epsilon [0\ 1000]\left(\frac{rad}{s}\right) for\ P_1 \epsilon \mathcal{P}_1, P_2 \epsilon \mathcal{P}_2 \tag{24}$$

Optimal tracking model of depth control system

For any structural uncertainty, the amplitude of the closed loop transfer function from input to output will be bounded between the following $b(\omega)$ and $a(\omega)$ functions

$$a(\omega) \le \left|F(s)\frac{P_{12}(s)G_1(s)}{1+P_{12}(s)G_1(s)}\right| \le b(\omega) \ , \quad \omega \le 1 for\ P_1 \epsilon \mathcal{P}_1, P_2 \epsilon \mathcal{P}_2$$

$$b(s) = \frac{\frac{\omega_{nU}^2}{a} \times (s+a)}{s^2 + 2\zeta_U \omega_{nU} s + \omega_{nU}^2} \ , \quad \omega_{nU} = 2.58\left(\frac{rad}{s}\right) \ , \ \zeta_U = 0.52 \ , \ a = 5 \tag{25}$$

$$a(s) = \frac{\omega_{nL}^2 \times b}{\left(s^2 + 2\zeta_L \omega_{nL} s + \omega_{nL}^2\right)(s+b)} \ ,$$

$$\omega_{nL} = 0.53\left(\frac{rad}{s}\right) \ , \ \zeta_L = 0.95 \ , \ b = 5$$

Output disturbance rejection

The output disturbance caused by the sea wave is considered in the form of a sine wave model and the output disturbance rejection model is considered as an exponential function. The frequency of sea waves in different marine conditions is less than one, therefore

$$\left|\frac{Z}{D}(j\omega)\right| = \left|\frac{1}{1+P_{12}(s)G_1(s)}\right| \le \left|\frac{1}{M(s)}\right|\left|\frac{1}{s+a}\right| ,$$

$$M(s) = \frac{cb}{s^2+b^2}, \ c = 0.5 \ , b = 0.84 \ , a = 1 \ , \quad \omega \epsilon [0\ \ 1]\left(\frac{rad}{s}\right) for\ P_1 \epsilon \mathcal{P}_1, P_2 \epsilon \mathcal{P}_2 \tag{26}$$

Input disturbance rejection

The surface control angle error can be considered as *V(t)=0.5* (deg). We want the ratio of the system response to input disturbance to be in the range of 0.6, therefore

$$\left|\frac{Z}{V}(j\omega)\right| = \left|\frac{\frac{P_{12}(s)}{G_2(s)}}{1+P_{12}(s)G_1(s)}\right| \le 0.6 \ , \quad \omega \epsilon [0\ 0.5]\left(\frac{rad}{s}\right) for\ P_1 \epsilon \mathcal{P}_1, P_2 \epsilon \mathcal{P}_2 \tag{27}$$

The PD gains for the inner pitch loop are tuned using loop shaping. In this step, a 20% error in determining the hydrodynamic coefficients is assumed as parametric uncertainty. The plant templates of the inner loop transfer function, G_θ , P_2 in Eq. (22), at different frequencies are shown in Fig. 7. Then, using only the constraint defined as the robust stability specification, Eq. (23), the stability bounds are obtained and loop shaping step, Fig. 8, is performed and the pitch controller is derived as follows

$$G_2(s) = \frac{\delta_s(s)}{e_\theta(s)} = -K_P\frac{(\tau_D s+1)}{(0.1\tau_D s+1)} = -1.3\frac{\left(\frac{1}{0.7}s+1\right)}{\left(0.1\frac{1}{0.7}s+1\right)} \tag{28}$$

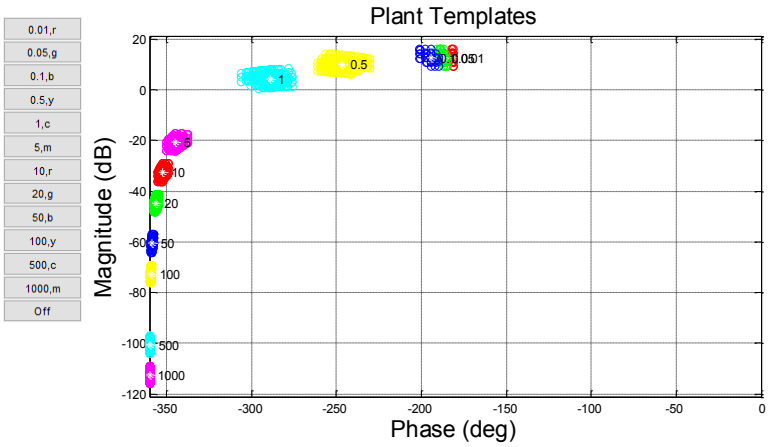

Fig. 7. Inner pitch control loop plant templates, p_2

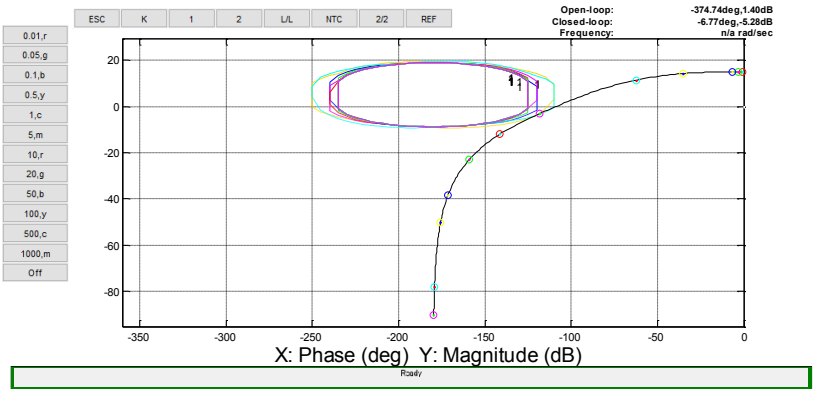

Fig. 8. Loop shaping step for inner pitch loop controller design, $G_2(s)$

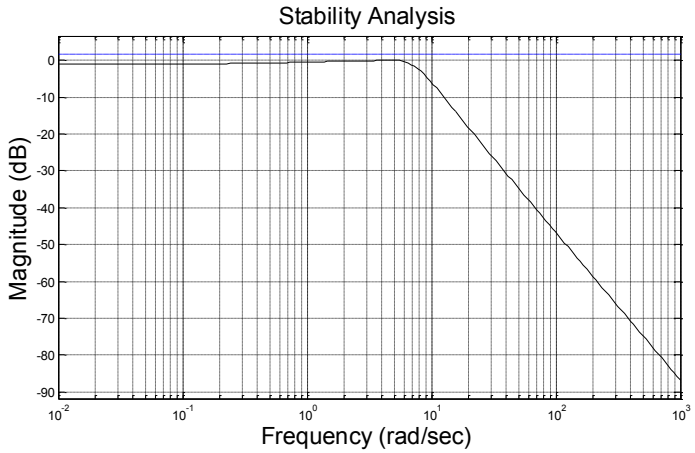

Fig. 9. Stability specification (blue dashed line) and maximum magnitude of the $\frac{P_2(s)G_2(s)}{1+P_2(s)G_2(s)}$ within the uncertain plants (black solid line) at each frequency

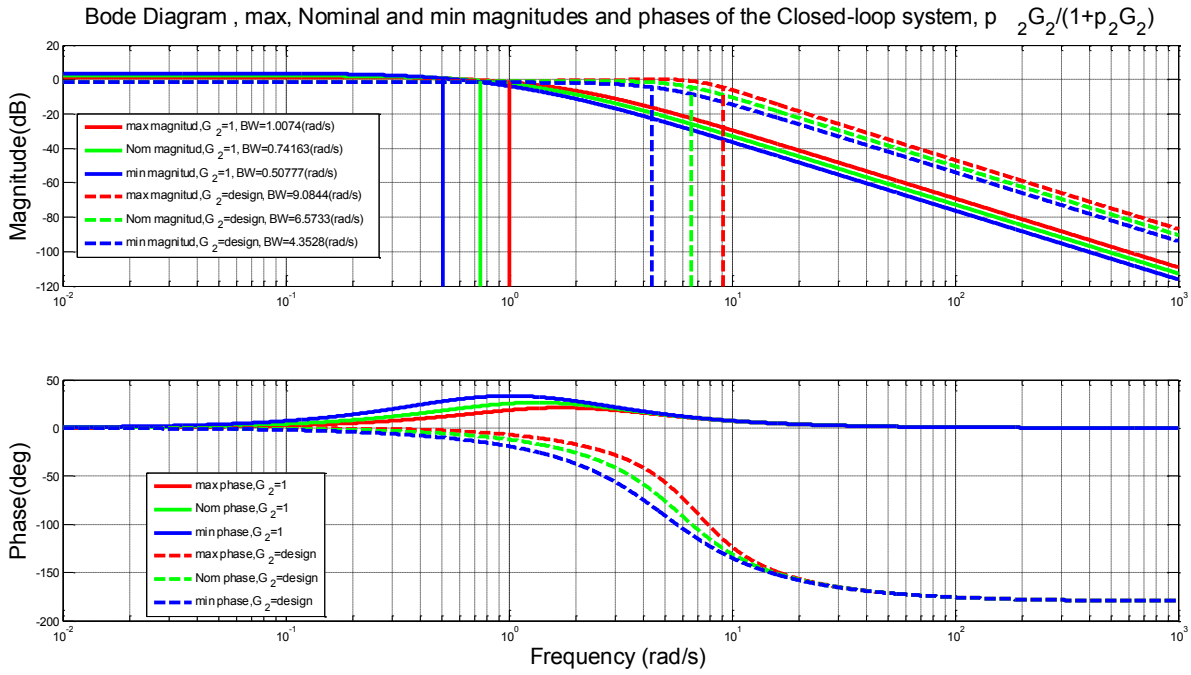

Fig. 10. The max, nominal and min magnitudes and phases of the closed-loop system, $\frac{P_2(s)G_2(s)}{1+P_2(s)G_2(s)}$, versus frequency (phase margin analysis), solid lines for G2 = 1, and dashed lines for designed G2

Stability analysis of the inner pitch loop considering the designed controller, Eq. (28), is shown in Fig. 9.

Fig. 10 shows the bandwidth of the inner pitch loop without a controller, $G_2 = 1$, and with the controller, G_2. Also, the phase margin for this loop with and without the controller for the maximum, nominal point, and minimum boundary created in the presence of a parametric uncertainty is shown in Fig. 11. As shown in Figs. 10 and 11, the dynamic of this system is inherently stable despite the structural uncertainty of both of the inner loop of the pitch and the outer loop of the depth, and the G_2 controller only improves the performance of the system for the ultimate target of the depth control. Therefore, the purpose of designing G_2, which is a PD controller, is to improve the depth regulation while maintaining the proper stability of the inner pitch loop, and thus, the desired P-PD control system is created.

By substituting $G_2(s)$ in $T_2(s)=\left|\frac{P_2(s)G_2(s)}{1+P_2(s)G_2(s)}\right|$ and considering $P_{12}(s)=T_2(s)P_1(s)$ as outer loop uncertain plant, we can design $G_1(s)$ by the QFT method to satisfy the corresponding defined constraints.

Since 20% error in hydrodynamic coefficients is considered as parametric uncertainty in the pitch transfer function and the 20% error due to the effect of ocean currents on velocity as parametric uncertainty in the depth transfer function, the plant templates of the outer control loop, G_2 , P_{12} in Eq. (22), are obtained as shown in Fig. 12. The stability bounds, based on Eq. (24), are obtained as shown in Fig. 13. Also, responses of the desired upper and lower bands of reference depth tracking, Eq. (25), to step input in the time domain are shown in Fig. 14 and its appropriate bounds due to parametric uncertainty in the Nichols chart are shown in Fig. 15. The disturbance rejection bounds for sea waves d the error bounds due to fin function as input disturbances, i.e. Eqs. (26) and (27), are obtained as in Figs. 16 and 17 in the Nichols chart, respectively. The intersection of the bounds is computed as shown in Fig. 18 and the control gain of the outer depth loop is tuned in the form of Eq. (29) using the QFT loop shaping rule as:

$$G_1(s)=\frac{\theta(s)}{e_Z(s)}=\gamma=-0.34 \tag{29}$$

Specification (blue dashed line) and maximum magnitude of the closed-loop transfer function within the uncertain plants (black solid line) for stability margin, reference depth input tracking, and input and output disturbance of the outer depth control loop considering the designed controller, Eq. (29), respectively are shown in Figs. 19 to 22.

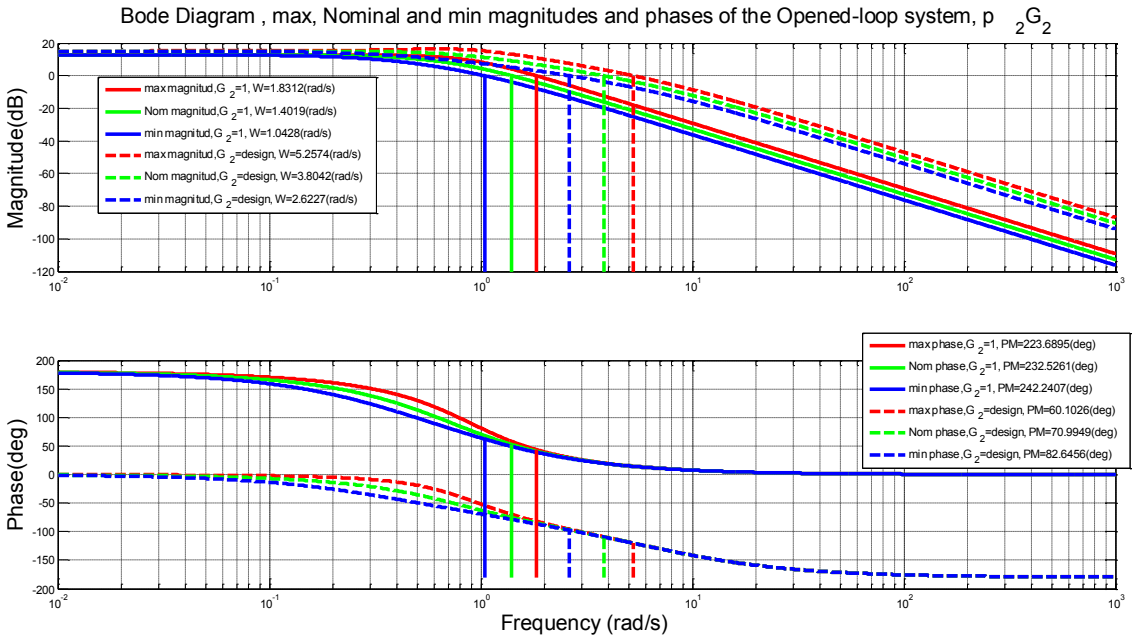

Fig. 11. The max, nominal and min magnitudes and phases of the opened-loop system, p2G2, versus frequency (phase margin analysis) solid lines for G2 = 1 and dashed lines for designed G2

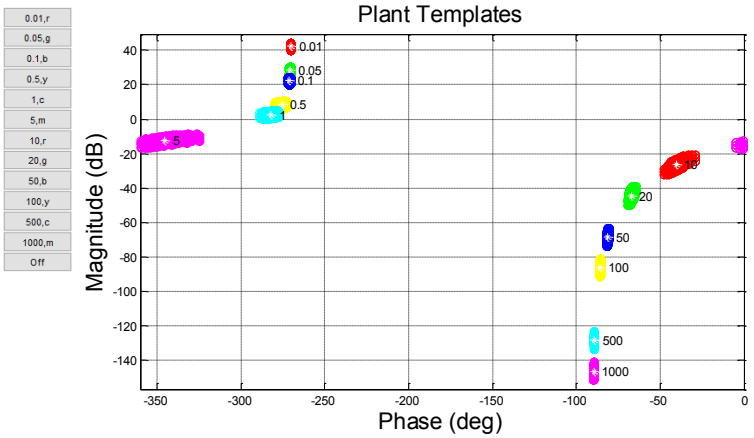

Fig. 12. Outer depth control loop plant templates, p_{12} .

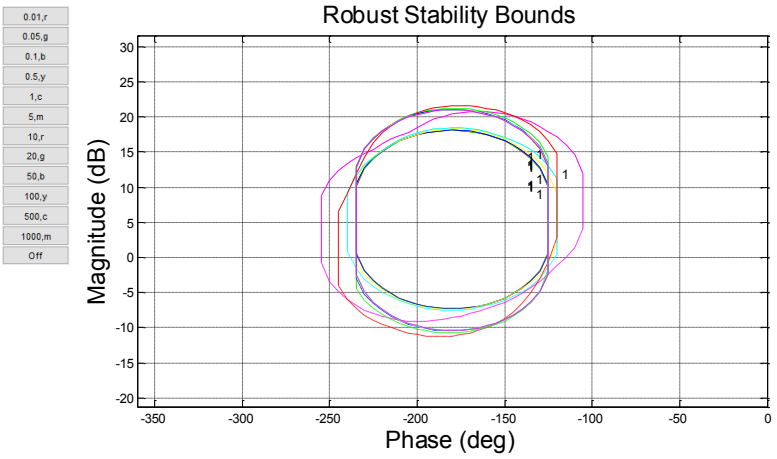

Fig. 13. Stability bounds of the outer depth control loop in the Nichols chart

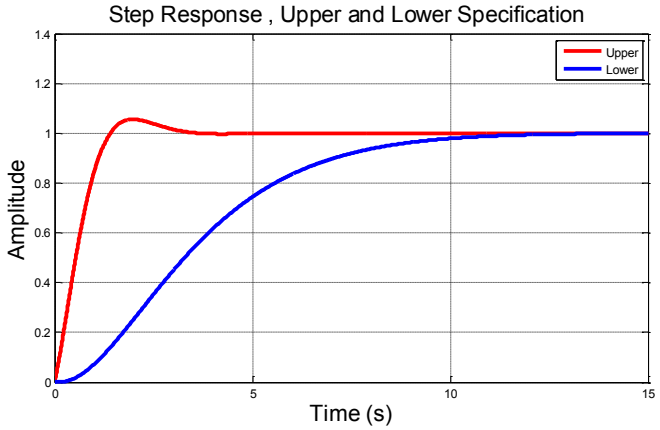

Fig. 14. Response of the upper and lower reference tracking models to step input

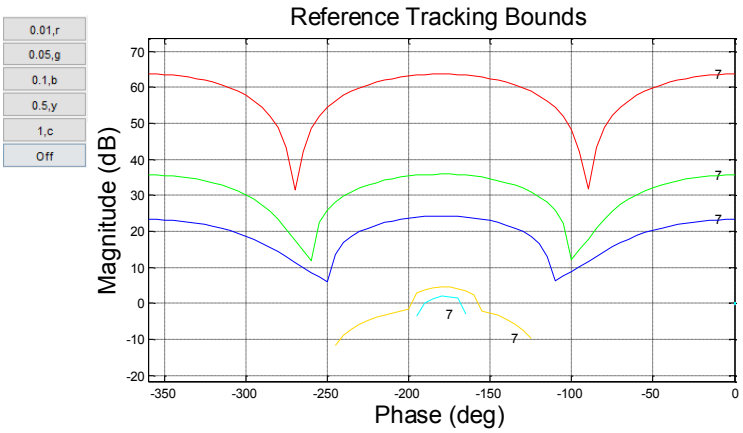

Fig. 15. Reference tracking bounds of the outer depth control loop in the Nichols chart

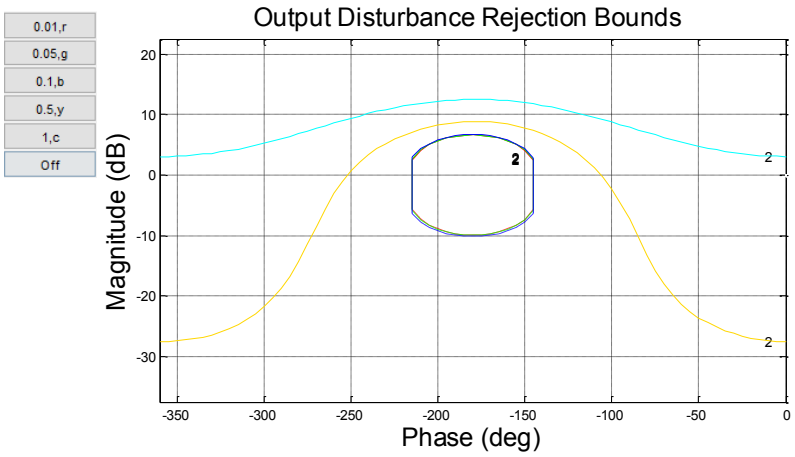

Fig. 16. Reference tracking bounds of the outer depth control loop in the Nichols chart

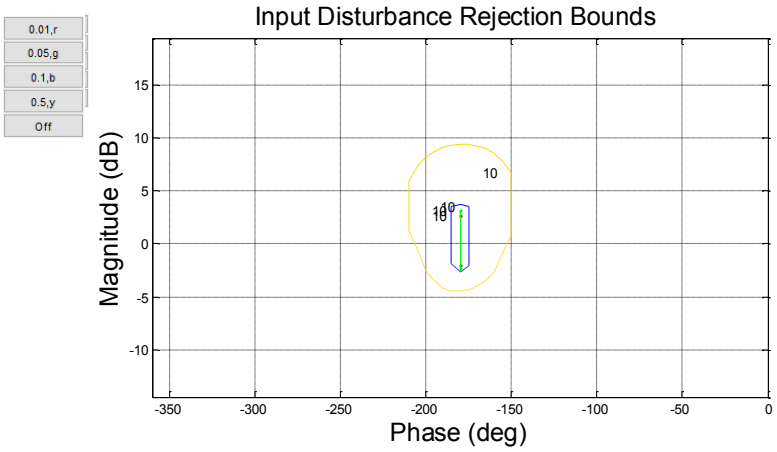

Fig. 17. Input disturbance rejection bounds of the outer depth control loop in the Nichols chart.

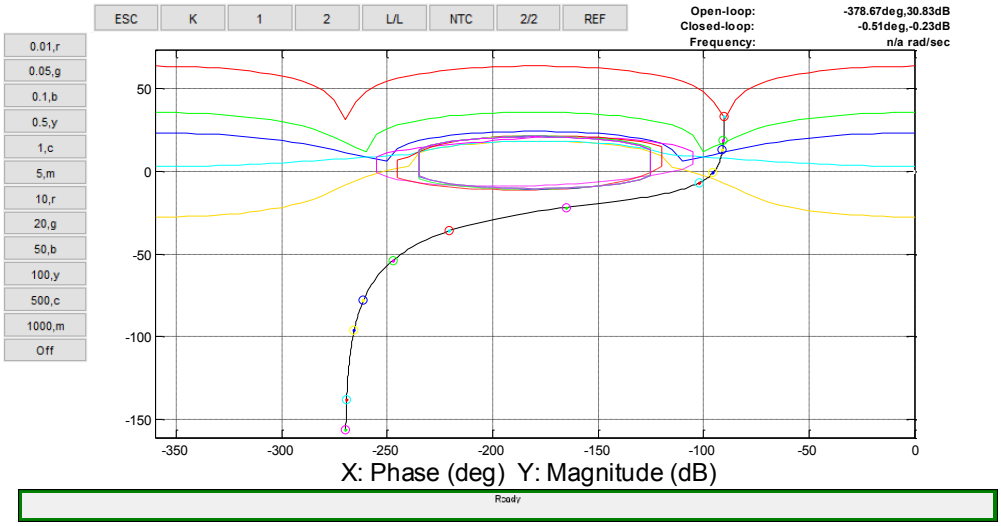

Fig. 18. Loop shaping of the outer loop controller for depth control, $G_1(s)$

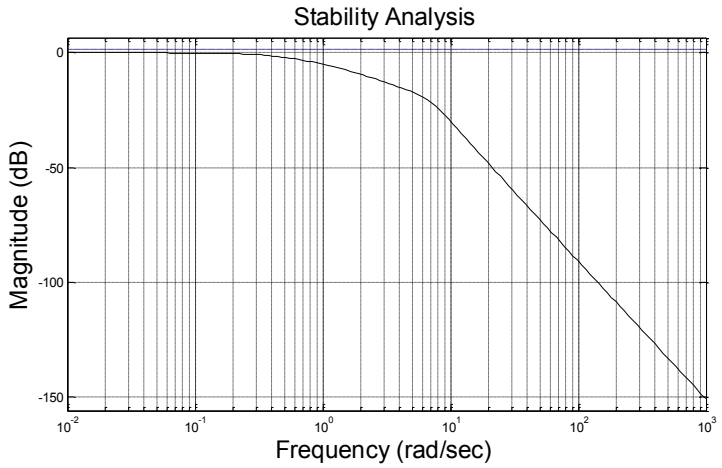

Fig. 19. Stability specification (blue dashed line) and maximum magnitude of the $\frac{P_{12}(s)G_1(s)}{1+P_{12}(s)G_1(s)}$ within the uncertain plants (black solid line) at each frequency

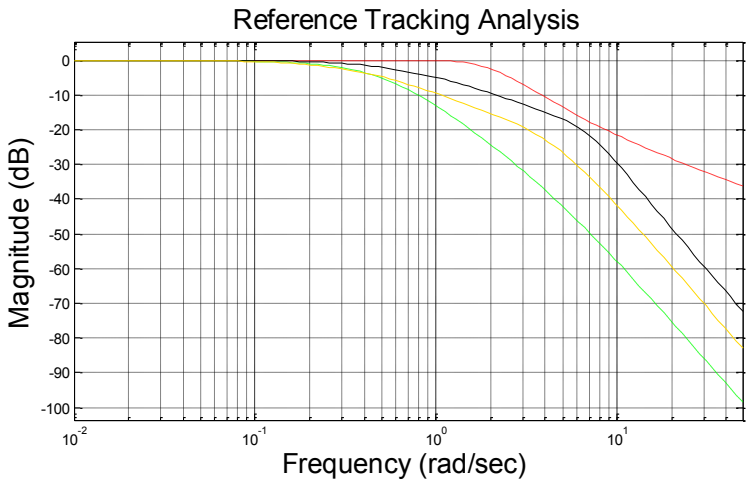

Fig. 20. Reference tracking specification (red and green dashed line) and maximum and minimum magnitude of the $F(s)\frac{P_{12}(s)G_1(s)}{1+P_{12}(s)G_1(s)}$ within the uncertain plants (black and yellow solid line) at each frequency

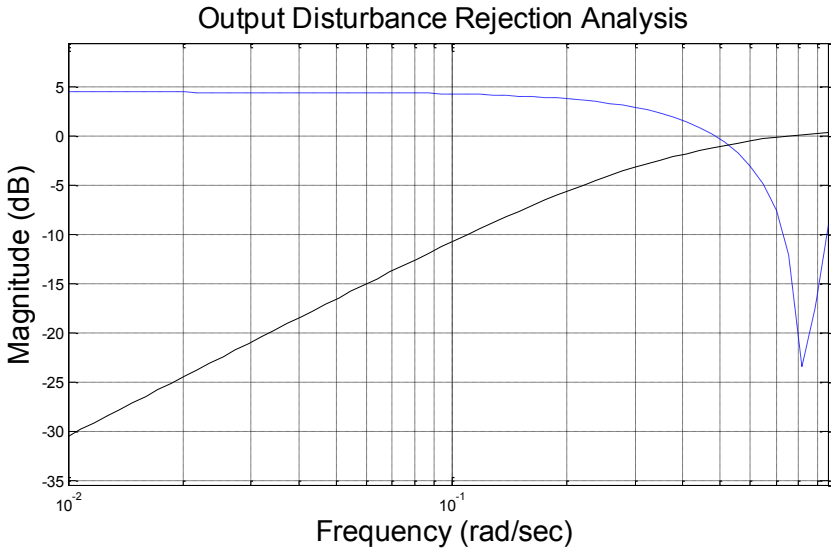

Fig. 21. Output disturbance rejection specification (blue dashed line), and maximum magnitude of the $\frac{1}{1+P_{12}(s)G_1(s)}$ within the uncertain plants (black solid line) at each frequency

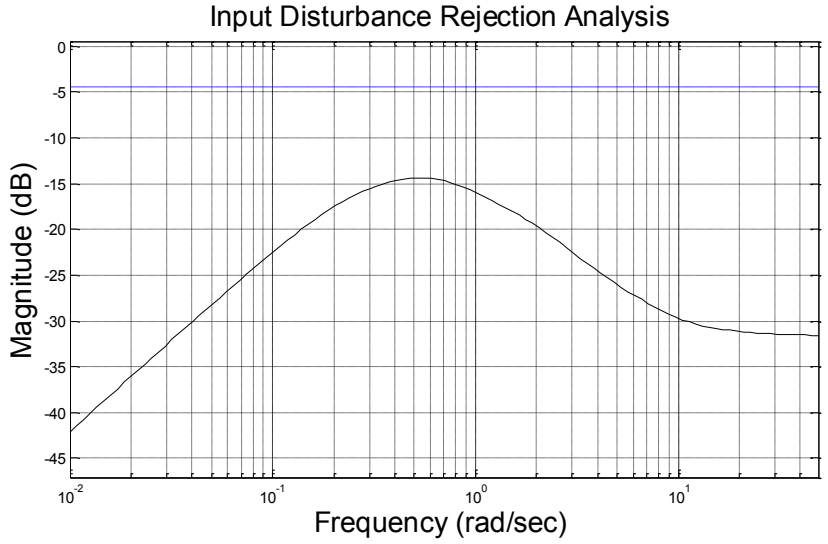

Fig. 22. Input disturbance rejection specification (blue dashed line) and maximum magnitude of the $\frac{\frac{P_{12}(s)}{G_2(s)}}{1+P_{12}(s)G_1(s)}$ within the uncertain plants (black solid line) at each frequency

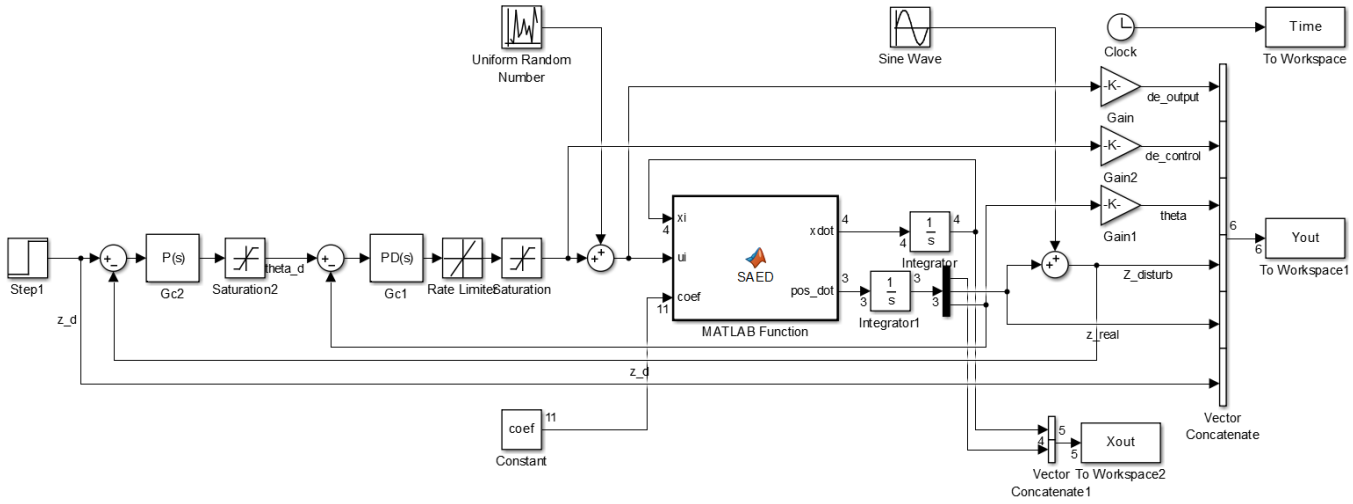

Fig. 23. Block diagram of the AUV control system in depth plane with sine wave output disturbance and random number as input disturbance in the fin error range

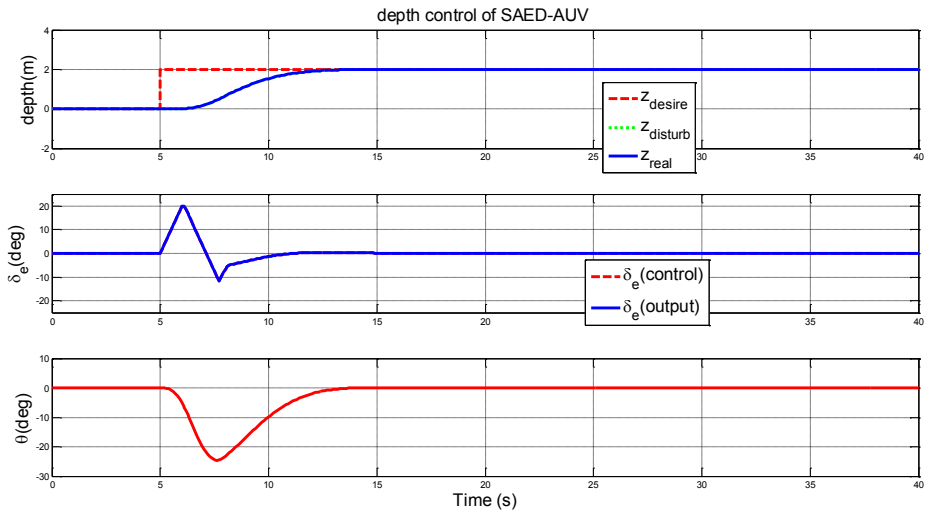

Fig. 24. AUV response to 2 m depth change without any disturbance to the system

4- Results and Discussion

In this section, using the Simulink toolbox of the MATLAB software, the results of the P-PD designed controller of the underwater vehicle SAED are simulated in the presence of parametric uncertainty and disturbances. In this research, the nonlinear equations of the AUV, i.e. Eq. (10), have been used as the real model of the SAED vehicle in the depth plane. As it was explained in previous sections, all design steps are based on linearized equations of motion but simulations will be examined on the nonlinear equations of motion because these conditions are more actual and the performance of the controllers will be known better.

The block diagram of the AUV control system in the depth plane despite the parametric uncertainty and the output disturbance as a sine wave and the input disturbance as a random number in the fin error range are shown in Fig. 23. In this simulation model, fin angle saturation in the range of ±20 deg and saturation rate of fin angle changes in the range of ±20 deg/sec have been accepted. To test the performance of the depth control system, various operating and environmental conditions that may occur during the movement of the vehicle in the depth plane are applied to the control system and responses of the vehicle are plotted.

Vehicle response and control system performance in tracking the reference depth input for different depths for nominal values of the vehicle model and without any disturbances are given in Figs. 24 to 26. It can be seen that the control system follows the reference input very well. This

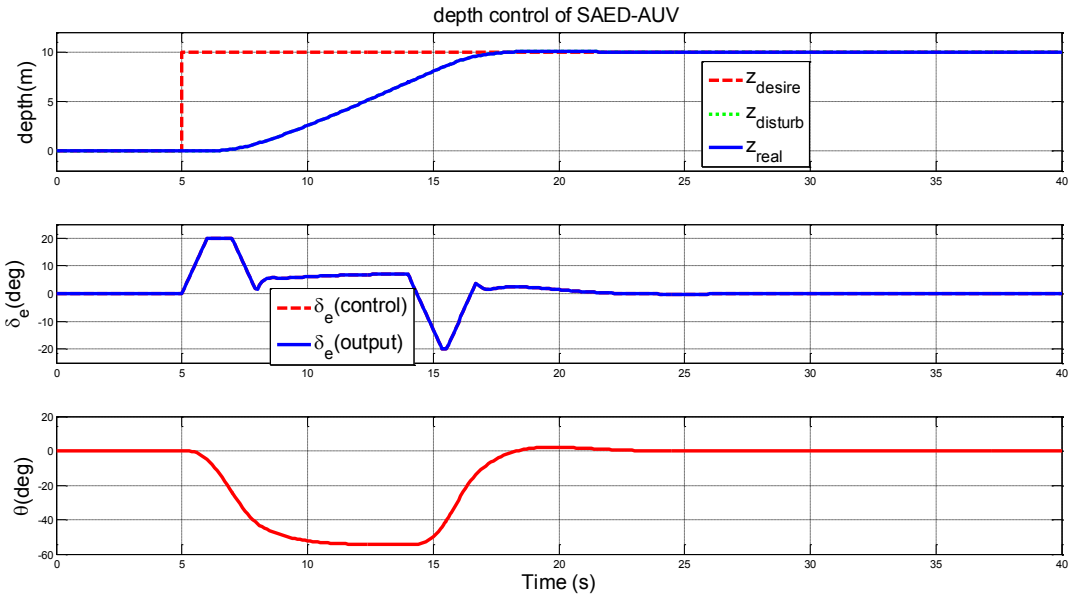

Fig. 25. AUV response to 10 m depth change without any disturbance to the system

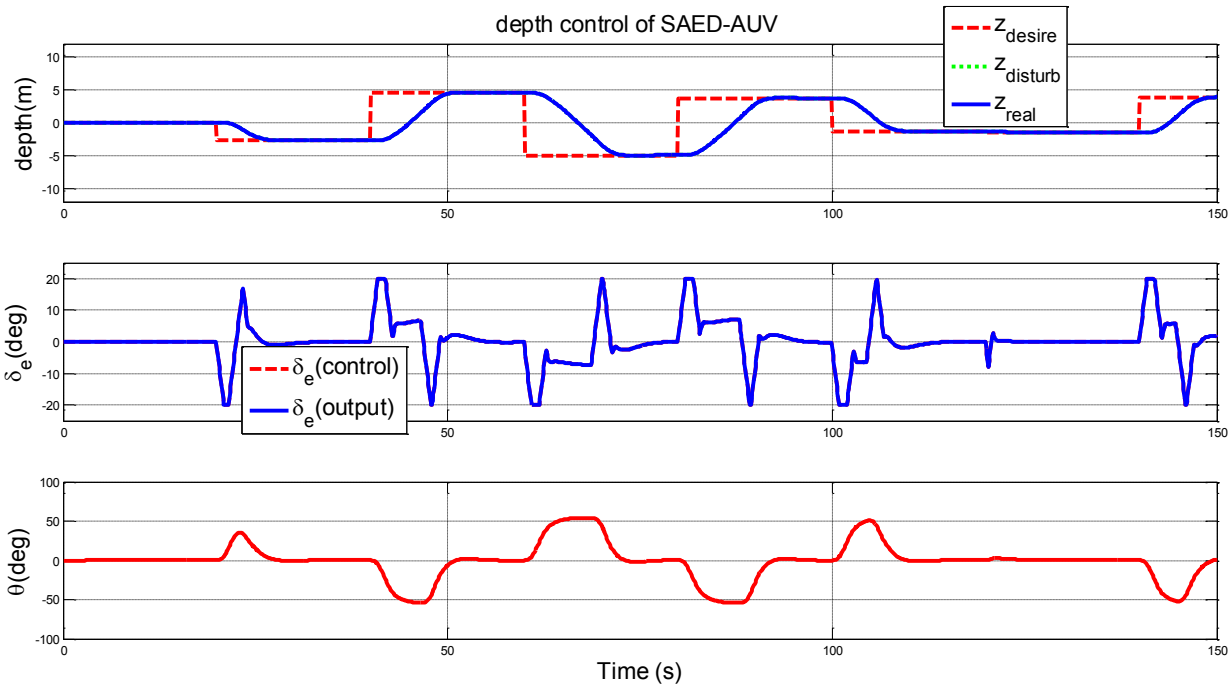

Fig. 26. Control system performance and AUV response to the depth change without any disturbance to the system

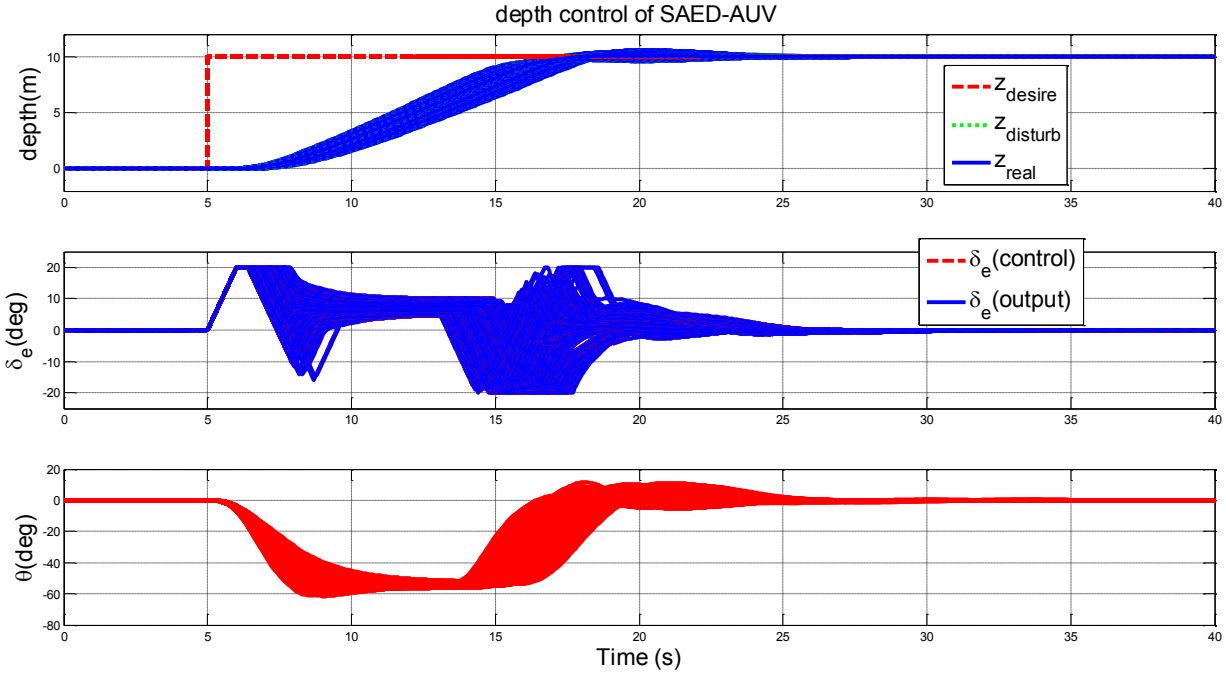

Fig. 27. Control system performance and AUV response to 10 m depth change despite parametric uncertainty and without any disturbance to the system

mode of operation is rather ideal, and therefore more realistic conditions will be taken into account in the next simulations.

Fig. 27 shows the performance of the control system in tracking the reference input for a parametric uncertainty range without any disturbances. To simulate the performance of the vehicle in real conditions, environmental disturbances and an error in the fin output angle are added to the control system. A random error in the ±1deg range of the fin angle is applied as the input disturbance to the system and the performance of the AUV control system in tracking the 10 m depth change reference input is simulated and shown in Fig. 28. Also, the effect of the sea wave as the output disturbance is applied to the system as a sinusoidal wave and the response of the system is simulated as in Fig. 29. Worst conditions, i.e. simultaneous presence of input and output disturbances, are shown in Fig. 30.

5- Conclusion

In this research, a robust P-PD controller was designed for an AUV using the QFT method in the presence of parametric uncertainty and input and output disturbances in depth plane motion. In the PID controller gain adjustment step, because the QFT method can consider parametric uncertainty, stability, and environmental and system disturbances simultaneously, then it may be concluded that this P-PD controller is a simple and applied controller for this system. The simulation results confirm using the QFT method in P-PD tuning for such a nonlinear system. Since other inputs were not studied in this paper, then the performance of the system with this special controller type to some possible inputs such as harmonic inputs, may not be good.

References

[1] Ö. Yildiz, R.B. Gökalp, A.E. Yilmaz, A review on motion control of the underwater vehicles, in: 2009 International Conference on Electrical and Electronics Engineering-ELECO 2009, IEEE, 2009, pp. II-337-II-341.

[2] S. Vahid, K. Javanmard, Modeling and control of autonomous underwater vehicle (AUV) in heading and depth attitude via PPD controller with state feedback, International Journal of Coastal and Offshore Engineering, 4 (2016) 11-18.

[3] S.D. Kadam, K.N. Tiwari, A simplified approach to tune PD controller for depth control of an autonomous underwater vehicle, in: proceedings of National conference on Communication, Computing and Networking Technologies, 2013, pp. 209-212.

[4] J. Guerrero, J. Torres, V. Creuze, A. Chemori, E. Campos, Saturation based nonlinear PID control for underwater vehicles: Design, stability analysis and experiments, Mechatronics, 61 (2019) 96-105.

[5] B. Subudhi, K. Mukherjee, S. Ghosh, A static output feedback control design for path following of autonomous

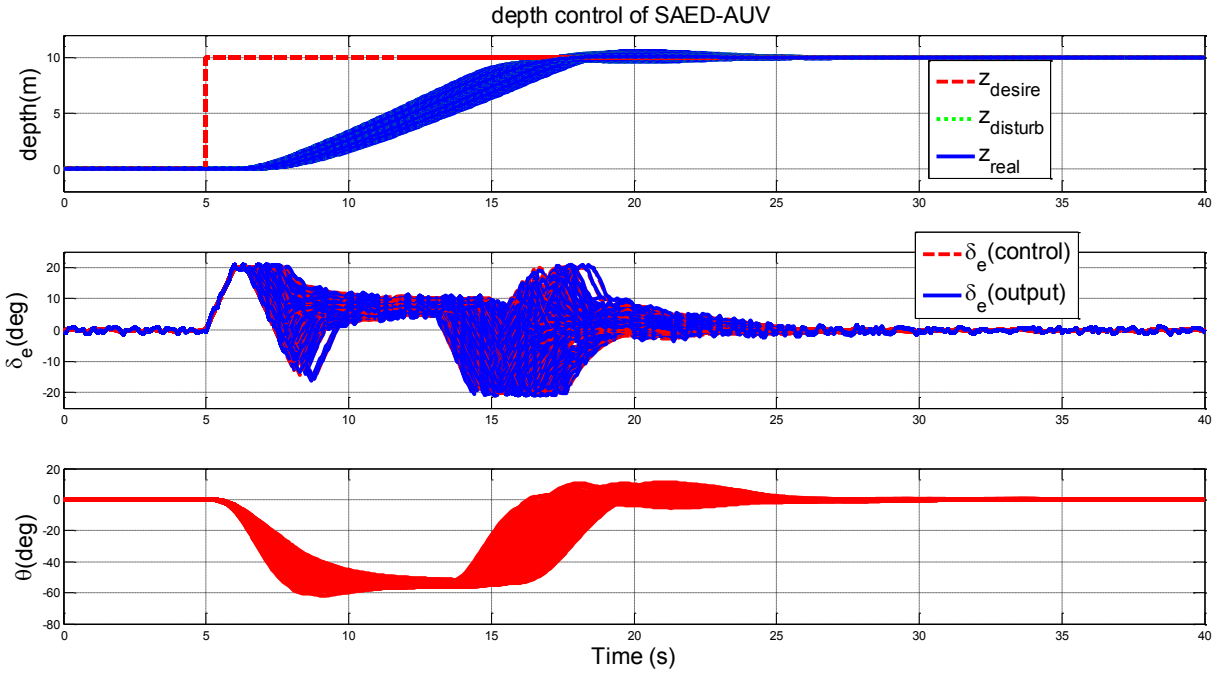

Fig. 28. Control system performance and AUV response to 10 m depth change despite both parametric uncertainty and input disturbance as a random error in the range of ±1deg fin angle

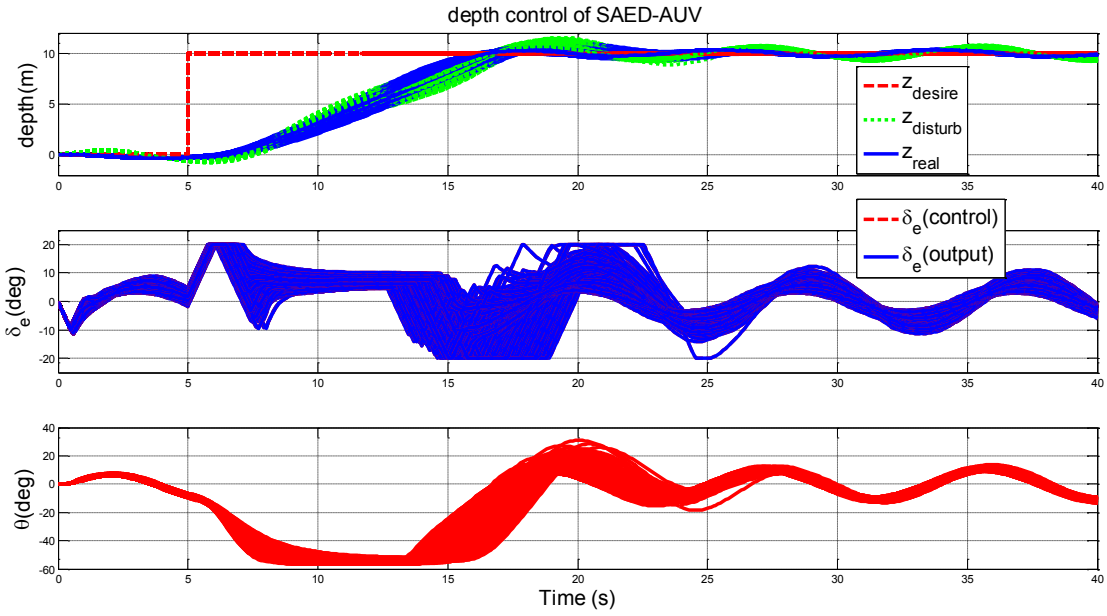

Fig. 29. Control system performance and AUV response to 10 m depth change despite both parametric uncertainty and output disturbance as a sine wave with a height of 1 m and a frequency of 0.74 rad/sec.

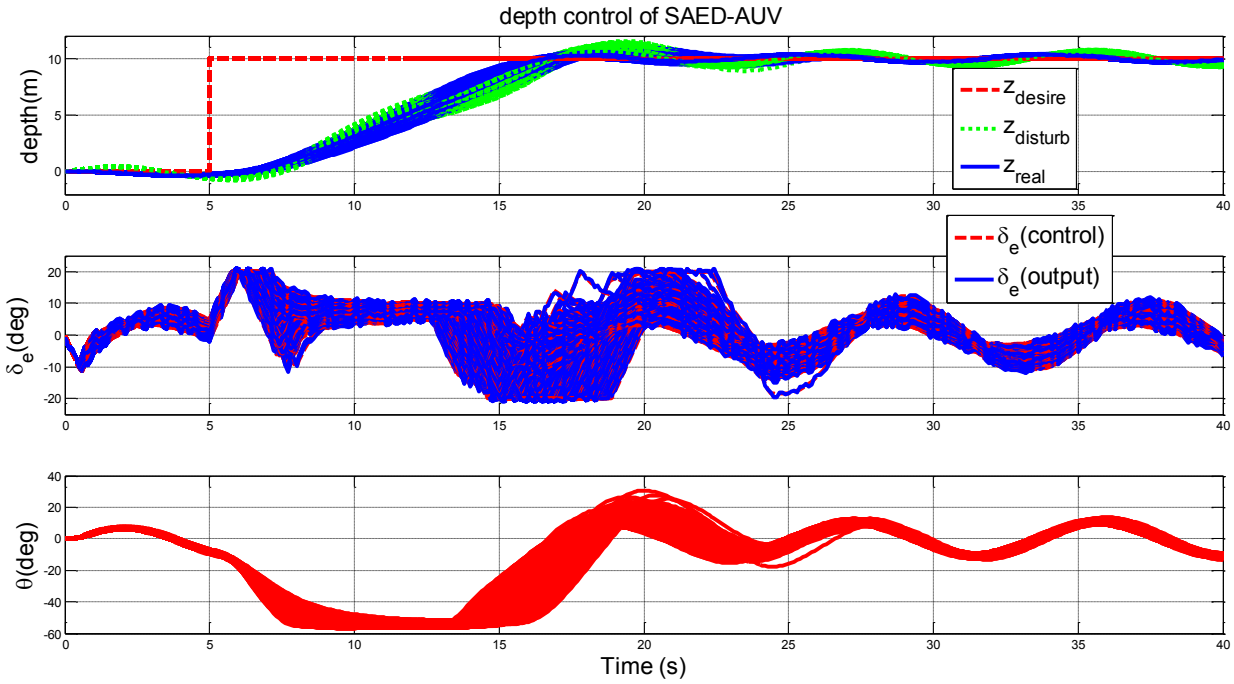

Fig. 30. Control system performance and AUV response to 10 m depth change despite parametric uncertainty and simultaneous existence of input disturbance as a random error in the range of ±1deg fin angle and output disturbance as a sine wave with a height of 1 m and frequency 0.74 rad/sec.

underwater vehicle in vertical plane, Ocean Engineering, 63 (2013) 72-76.

[6] R. Cui, X. Zhang, D. Cui, Adaptive sliding-mode attitude control for autonomous underwater vehicles with input nonlinearities, Ocean Engineering, 123 (2016) 45-54.

[7] N.-H. Tran, T.-P. Tran, T.-P. Ton, Design Depth Controller for Hybrid Autonomous Underwater Vehicle using Backstepping Approach, in: 2020 5th International Conference on Green Technology and Sustainable Development (GTSD), IEEE, 2020, pp. 424-429.

[8] F. Yao, C. Yang, X. Liu, M. Zhang, Experimental evaluation on depth control using improved model predictive control for autonomous underwater vehicle (AUVs), Sensors, 18(7) (2018) 2321.

[9] K.W. Lee, S.N. Singh, Nonlinear adaptive trajectory control of multi-input multi-output submarines with input constraints, Proceedings of the Institution of Mechanical Engineers, Part I: Journal of Systems and Control Engineering, 230(2) (2016) 164-183.

[10] Y. Wang, Y. Shen, K. Wang, Q. Sha, B. He, T. Yan, Fuzzy controller used smoothing function for depth control of autonomous underwater vehicle, in: OCEANS 2016-Shanghai, IEEE, 2016, pp. 1-5.

[11] Z. Chu, D. Zhu, G.E. Jan, Observer-based adaptive neural network control for a class of remotely operated vehicles, Ocean Engineering, 127 (2016) 82-89.

[12] J. Wan, B. He, D. Wang, T. Yan, Y. Shen, Fractional-order PID motion control for AUV using cloud-model-based quantum genetic algorithm, IEEE Access, 7 (2019) 124828-124843.

[13] L. Zhang, L. Zhang, S. Liu, J. Zhou, C. Papavassiliou, Low-level control technology of micro autonomous underwater vehicle based on intelligent computing, Cluster Computing, 22(4) (2019) 8569-8580.

[14] A. Sahoo, S.K. Dwivedy, P. Robi, Adaptive Fuzzy PID Controller for A Compact Autonomous Underwater Vehicle, in: Global Oceans 2020: Singapore–US Gulf Coast, IEEE, 2020, pp. 1-6.

[15] M.M. Hammad, A.K. Elshenawy, M. El Singaby, Trajectory following and stabilization control of fully actuated AUV using inverse kinematics and self-tuning fuzzy PID, PloS one, 12(7) (2017) e0179611.

[16] N.Q. Hoang, E. Kreuzer, Adaptive PD-controller for positioning of a remotely operated vehicle close to an underwater structure: Theory and experiments, Control engineering practice, 15(4) (2007) 411-419.

[17] A.C. Zolotas, G. Halikias, Optimal design of PID controllers using the QFT method, IEE Proceedings-Control Theory and Applications, 146(6) (1999) 585-589.

[18] M.R. Gharib, M. Moavenian, Synthesis of robust PID controller for controlling a single input single output

system using quantitative feedback theory technique, Scientia Iranica. Transaction B, Mechanical Engineering, 21(6) (2014) 1861-1869.

[19] R. Comasolivas, T. Escobet, J. Quevedo, Automatic design of robust PID controllers based on QFT specifications, IFAC Proceedings Volumes, 45(3) (2012) 715-720.

[20] M.D. Patil, K.R. Kothawale, Design of robust PID controller for flexible transmission system using quantitative feedback theory (QFT), in: International Conference on Advances in Computing, Communication and Control, Springer, 2011, pp. 479-485.

[21] T.T.J. Prestero, Verification of a six-degree of freedom simulation model for the REMUS autonomous underwater vehicle, Massachusetts institute of technology, 2001.

[22] D. Myring, A theoretical study of body drag in subcritical axisymmetric flow, Aeronautical quarterly, 27(3) (1976) 186-194.

HOW TO CITE THIS ARTICLE

F. Safari, M. Rafeeyan, M. Danesh, Design of Robust Proportional-(Proportional-Derivative) Controller for an Autonomous Underwater Vehicle Using Quantitative Feedback Theory in the Diving Plane, AUT J. Mech Eng., 6(3) (2022) 363-386.

DOI: 10.22060/ajme.2022.20964.6026